Insertion of Oxygen and Nitrogen in the Siliceous Zeolite TON at High Pressure

Mario Santoro, Marta Morana, Demetrio Scelta, Jérôme Rouquette, Kamil Dziubek, Federico Gorelli, Roberto Bini, Gaston Garbarino, Arie van Der Lee, Francesco Di Renzo, et al.

Insertion of Oxygen and Nitrogen in the Siliceous Zeolite TON at High-Pressure

Mario Santoro[‡,§], Marta Morana[§,ǁ], Demetrio Scelta[ǁ,§], Jérôme Rouquette[†], Kamil Dziubek[§,¶], Federico A. Gorelli[‡,§], Roberto Bini[§▲], Gaston Garbarino[⊥], Arie van der Lee[▽], Francesco Di Renzo[†], Benoît Coasne[□], Julien Haines*[†]

[‡]Istituto Nazionale di Ottica, CNR-INO, 50019 Sesto Fiorentino, Italy.

[§]European Laboratory for Non Linear Spectroscopy (LENS), 50019 Sesto Fiorentino, Italy.

[ǁ]ICCOM-CNR, Institute of Chemistry of OrganoMetallic Compounds, National Research Council of Italy, Via Madonna del Piano 10, I-50019 Sesto Fiorentino, Firenze, Italy.

¶ Faculty of Chemistry, Adam Mickiewicz University, Uniwersytetu Poznańskiego 8, 61-614 Poznań, Poland

[†]ICGM, CNRS, Université de Montpellier, ENSCM, 34095 Montpellier, France.

[▲]Dipartimento di Chimica "Ugo Schiff" Università di Firenze – 50019 Sesto Fiorentino - Italy

[⊥]ESRF, 38000 Grenoble, France.

[▽] IEM, CNRS, Université de Montpellier, 34095 Montpellier, France

[□] Université Grenoble Alpes, CNRS, LIPhy, 38000 Grenoble, France

Supporting Information Placeholder

ABSTRACT

The insertion of oxygen and nitrogen molecules in the 1D pore system of the zeolite TON was studied at high pressure by vibrational spectroscopy, x-ray diffraction and by Monte Carlo (MC) molecular modelling. Rietveld refinements and MC modelling indicate that on average six diatomic molecules per unit cell enter the pores of the zeolite. This induces changes in compressibility and distortion related to the *Cmc*2_1 to a *Pbn*2_1 phase transition compared to the empty-pore material. The filling behavior with N_2 and O_2 under pressure is similar to that of argon, suggesting that the kinetic diameter, which is very close in these three systems, plays a major role. The orientation of the diatomic molecules appears to have a rather minor effect on filling occurring at a slightly higher pressure for N_2, which has a larger kinetic diameter. Both inserted molecules, initially not showing any marked orientation, begin to exhibit a degree of orientational order above 2 GPa.

1. Introduction

Zeolites are natural or synthetic aluminosilicates built up of corner-sharing TO_4 (T = Si, Al…) tetrahedra, which form a network of pores with typical diameters between 3 and 8 Å. These microporous materials are used at a large scale for applications in, for example, catalysis, adsorption, separation and ion exchange. In the recent years, we conducted several foundational studies on the high pressure (GPa) insertion of simple molecular systems into inert, purely siliceous zeolites, with an at least twofold purpose[1-11]. On one hand, we aimed to obtain sub-nanophases of densely confined guest simple systems in the host zeolites and to compare the intermolecular interactions and distances in the confined matter to those of the corresponding bulk systems at the same pressures. These interactions were indeed found to be very similar in the two cases, thereby providing a rationale and also a guide for tailoring potential pressure induced chemical reactions in this sort of confined molecular matter[9]. On the other hand, we aimed to obtain purely pressure induced chemical reactions such as the polymerization, in the case of simple C-based molecules as the guest species. In this case, novel hybrid organic/inorganic, polymer/zeolites sub-nanocomposites were synthesized and recovered at ambient conditions[5-8], a class of materials which may exhibit a rich diversity of physical properties suitable for potential applications in modern micro-electronics/photonics/mechanics and energy storage. In this context, we note that these studies are connected to high-pressure effects that have been proposed to rationalize strong confinement effects on catalytic reactions and/or phase transitions[12-13].

One crucial, fundamental aspect in this research is the understanding of how the degree of filling of the inserted molecules depends on pressure and also how the structure of the host zeolite is affected. These two aspects were quantitatively investigated by means of X-ray diffraction on the purely SiO_2 zeolite ZSM-22 (TON) filled by Ne and Ar[10]. TON is a 1D micro-channel system based on 10-membered rings of SiO_4 tetrahedra with elliptical cross sections of 5.7 Å and 4.6 Å, respectively[14]. The insertion of the rare gas systems was found to strongly depend on the van der Waals (vdW) radius, equal to 1.5 Å and 1.8 Å in Ne and Ar, respectively, thereby differing by about 18%. Ne was found to completely fill the pores of TON at 4 GPa, achieving the saturation value of 12 Ne atoms per unit cell of the host zeolite, whereas

the degree of filling with Ar was almost two times lower. Also, the compressibility and structural distortions, such as pore ellipticity, are considerably reduced in the case of Ne as compared to the argon-filled and the empty pore material[15].

In this work, we aim to provide a more general view on pressure driven filling of TON by extending our investigation to the case of the insertion of the simplest possible molecular systems possessing orientational degrees of freedom: the homonuclear diatomic molecules. Specifically, we chose N_2 and O_2 as the test systems, since the high pressure phase diagram of these two bulk substances, which we use as a reference here, is well known in the literature[16-30]. The present study on confined N_2 and O_2 in TON is based on Raman spectroscopy, X-ray diffraction, and Monte Carlo (MC) molecular modeling in the 0-20 GPa pressure range.

2. Experimental and theoretical methods

The TON sample was prepared by sol-gel techniques using triethylenetetramine as the structure directing agent followed by crystallization at 170°C under hydrothermal conditions and then calcination at 600°C[15, 31-32]. Samples were prepared in which either oxygen or nitrogen was loaded with micron/submicron-size TON powder in stainless steel gasketed diamond anvil cells (DACs), with typical initial sample dimensions of 150-320 μm in diameter and 40-50 μm in thickness. We first homogeneously filled the gasket hole by TON powder and the powder was just gently compacted in order not to prevent the subsequent loading of the condensed gases. Either O_2 or N_2 was then loaded cryogenically at 77 K in its liquid phase at about 1 bar, and the liquid filled both the pores of the zeolite (confined O_2 and N_2) and residual empty space between the grains of TON (bulk O_2 and N_2). These samples were used for *in situ* Raman spectroscopy and X-ray diffraction (XRD) investigations under pressure. Ruby chips were inserted in the samples and pressure was measured based on the shift of the ruby R_1 fluorescence line[33]. Raman signals were excited by the 647.1 nm line of a Kr^+ laser. Backscattering geometry was used through a 20× Mitutoyo

micro-objective providing a beam spot of 2-3 μm, and the scattered light was detected by a single monochromator (Acton/SpectraPro 2500i) equipped with super notch filters and a CCD detector (Princeton Instruments Spec-10:100BR)[34] with typical spectral resolution of 0.6 cm^{-1}.

X-ray diffraction (λ=0.41121 Å) was performed in a diamond anvil cell (DAC) on beamline ID15B at the ESRF synchrotron using a MAR555 flat panel detector. The nominal size of the focal spot was 30 μm. The diffraction patterns were analyzed and integrated using the FIT2D program[35]. Rietveld refinements were performed using the program Fullprof[36]. Soft constraints were applied to the Si-O distances, O-O distances and/or the O-Si-O angles. Crystal structures were plotted using the program VESTA[37].

Monte Carlo simulations in the Grand Canonical ensemble (GCMC) were performed to determine the number, the positions and orientations of O_2 and N_2 confined at room temperature in TON. Such atom-scale simulations at constant chemical potential μ, volume V, and temperature T allow determining the number of adsorbed oxygen, $n_{O2}(\mu)$, and nitrogen, $n_{N2}(\mu)$, molecules per zeolite unit cell as a function of chemical potential μ[38]. For a given μ and T, the corresponding pressure P was obtained according to the following strategy[39-40]. We perform GCMC simulations of bulk O_2 and bulk N_2 to obtain the relationship between chemical potential μ and density, $\rho(\mu)$. On the other hand, the relationship $\rho(P)$ between pressure P and density ρ is determined using Monte Carlo simulations in the isobaric-isothermal ensemble (NPT). From $\rho(\mu)$ and $\rho(P)$, $\mu(P)$ can be determined readily. For each gas, the pressures (or chemical potential) and unit cell parameters obtained from the experiments were used to perform these molecular simulations. A TON structure made of 2 × 2 × 5 rigid unit cells was considered and periodic boundary conditions were used along the x, y, z directions to avoid finite size effects. O_2 and N_2 were described in these atom-scale simulations using all-atom potentials from the TRAPPE force field[41-42]. In more detail, for these two molecules, each atomic site is a Lennard-Jones center with the following parameters: σ = 0.302 nm, ε/k_B = 49 K for the O atom in O_2 and σ = 0.331 nm, ε/k_B = 36 K for the N atom in N_2. In addition, to describe the electric quadrupole moment, each of these atomic sites carries a partial charge; q_O = -0.113e and q_N = -0.482e (the bond length is set to 0.11 nm for N_2 and 0.121 nm for O_2). For each molecule, to ensure

charge neutrality, the center of mass carries a charge -2q. Interactions with the O and Si atoms of zeolite TON were also described using the Lennard – Jones potential and the Coulomb electrostatic potential. The cross parameters σ and ε were determined by combining the like-atom parameters using the Lorentz – Berthelot rules (the like-atom parameters for zeolite TON are $\sigma = 0.3795$ nm, $\varepsilon/k_B = 64.2$ K for Si and $\sigma = 0.3154$ nm, $\varepsilon/k_B = 78.0$ K for O). As for the electrostatic charges on the Si and O atoms of the zeolite, there are taken from the force field for silica by Carre et al.[43]

3. Results and discussion

Raman spectra of the molecular stretching were measured up to about 20 GPa on O_2/TON and N_2/TON mixtures, respectively (figure 1). In all cases, close to the peaks for the bulk systems, other much weaker yet clearly visible peaks appear, which we easily assign to confined O_2 and N_2. In the O_2/TON mixture at 0.5 GPa, we observe one single peak for confined O_2, and the two peaks of confined and bulk O_2 are rather sharp and well separated with the peak for confined O_2 positioned at slightly lower frequencies. Both peaks then suddenly broaden upon increasing pressure up to about 5.5 GPa, and the peak for confined O_2 appears as a not resolved, low frequency shoulder of the much sharper bulk O_2 peak. Above 5.5 GPa, bulk oxygen solidifies (β phase) and the corresponding peak sharpens significantly, while the peak for confined O_2 remains quite broad and much better distinguishable from the peak of the bulk phase. Above 10 GPa, at the δ-ε phase transition for pure O_2, the bulk O_2 peak jumps down to lower frequencies, due the formation of weakly bonded $(O_2)_4$ tetramers, which are the molecular units of the ε phase. Correspondingly, confined oxygen displays two distinct peaks, slightly sharper than those observed below 10 GPa, now positioned at higher frequencies with respect to the peak of pure oxygen, which originate from weakly bonded $(O_2)_2$ dimers mixed with monomeric units both forming the confined material, as shown by us recently[44]. In N_2/TON mixtures, we observe two distinct peaks for confined nitrogen at 2.8 GPa, at slightly lower and higher frequencies, respectively, with respect to the much stronger single peak of solid bulk nitrogen indicating that we have at least two symmetry independent molecules per unit cell. Upon

increasing pressure, the two peaks for confined nitrogen become more separated, but also increasingly broader, while solid nitrogen displays the sharp ν_1 and ν_2 peaks, in both δ and ε phase.

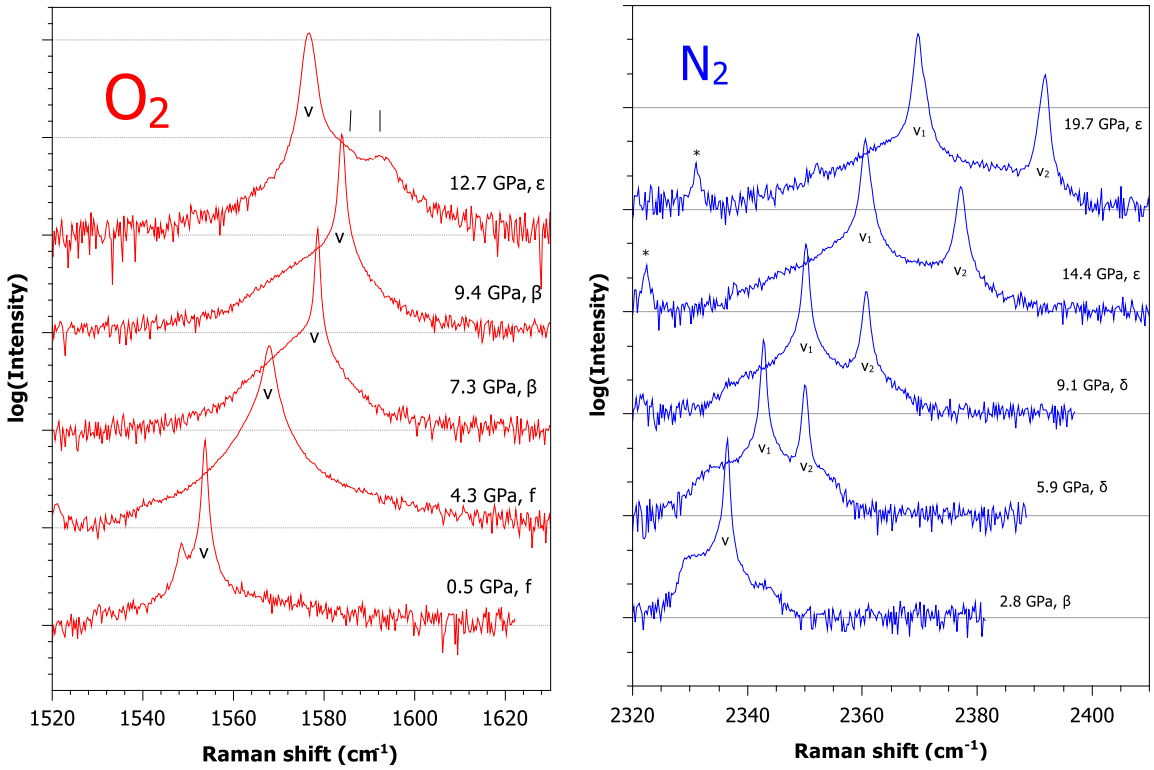

Figure 1. Selected Raman spectra of O_2 /TON and N_2 /TON mixtures measured upon increasing pressure. Logarithm (log) of the intensity is reported on the vertical scale. The spectra have been also vertically shifted, for the sake of visual clarity. Greek letters β, δ, and ε, and "f": solid phases and the fluid phase, respectively. The ν, ν_1 and ν_2 letters indicate the crystalline components for the molecular stretching in the bulk phases. Vertical bars in the left panel indicate two distinct stretching modes for confined oxygen, which appear above 10 GPa (see main text). Asterisks in the right panel indicate the isotopic $^{15}N^{14}N$ stretching peak.

Our spectroscopic investigation allows us to draw a few important observations on the inserted molecular systems. Firstly, pressure shift of frequency for the confined and bulk systems are roughly similar. Also, at least for nitrogen, where two crystalline components are observed above 5.0 GPa in the pure system with a frequency spread that increases with pressure, we observe that the pressure behavior of the

frequency spread for the confined and bulk systems are very similar to one another. These facts suggest that intermolecular interactions and, as a consequence, intermolecular distances are very similar in the two cases, the confined and the bulk system, as already observed by us in the O_2/TON and the N_2/silicalite systems[9, 44]. A second important observation deals with the confined systems displaying two Raman peaks, clearly visible for oxygen above 10 GPa and for nitrogen starting from low pressure. This is a first hint that at least two crystallographically independent, inserted molecules should sit within the primitive cell of TON. This finding is quantitatively assessed below, by the XRD investigation. A third very important outcome from the Raman studies stems from the pressure behavior of the integrated, total intensity ratio for confined O_2 and N_2, normalized to the integrated intensity for the bulk peak (in the case of N_2, only the ν_1 peak was considered above 5.0 GPa). These intensities have been obtained after a fitting procedure of the measured peaks to pseudo-Voigt functions. In figure 2, we report the normalized intensity for confined O_2 and N_2 vs. pressure up to 10 GPa, which is the range of pressures where Rietveld refinements of our XRD data are also available for a quantitative comparison. Incidentally, in the case of oxygen, we note that although the Raman intensity can change upon pressure increase because of changes in the molecular electronic structure [ref. 17-18], the normalized quantity reported in figure 3 should not be affected by these changes, which indeed reasonably occur for confined and bulk oxygen to the same extent. The normalized intensity for the confined matter clearly increases upon increasing pressure, reaching a sort of saturation above 3-4 GPa. Fitting of data points to an empirical increasing exponential function: $A[1\text{-}\exp(-P/P_r)]$, leads to a typical pressure grow rate of P_r=1.8 GPa. It is very straightforward to assign this type of growing mainly to the increasing number of inserted molecules with pressure in the host zeolite, a result which is quantitatively confirmed below by XRD.

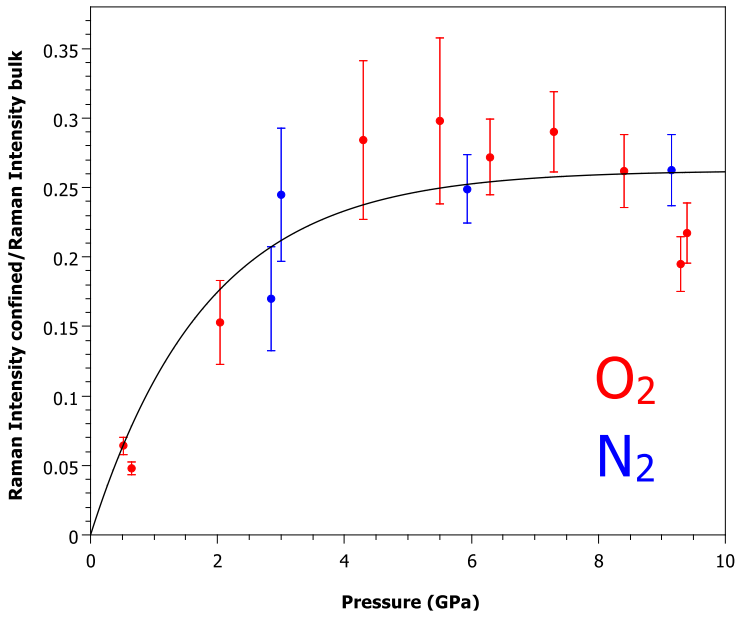

Figure 2. Red and blue circles: integrated Raman intensity for confined O_2 (red) and N_2 (blue) normalized to the integrated intensity for the corresponding bulk systems, see text. Points for N_2 have been vertically rescaled by a factor of 1.36 in order to display the same average value as those for O_2 above 4.0 GPa. An increasing exponential function was fitted to the whole set of data: $A[1\text{-}\exp(-P/P_r)]$, with A=0.26 and P_r=1.8 GPa.

Powder XRD patterns were measured up to 20 GPa on TON in oxygen and in nitrogen. The data obtained above 10 GPa for oxygen were subject to extremely strong contamination from the diffraction due to bulk ε-oxygen. In both cases changes in relative intensity were observed due to pore filling and TON remained crystalline up to the highest pressure reached, Figure 3. Rietveld refinements were performed up to 10 GPa for both systems, which except for the lowest pressure point at 0.45 GPa in the TON-O_2 experiment, correspond to the high pressure $Pbn2_1$ phase of TON. Fourier difference maps were calculated. Strong peaks were found in the pores and these peaks were used to place the guest molecules in the unit cell, which were modelled using isoelectronic silicon and sulfur atoms for N_2 and O_2 molecules, respectively. The results indicate that the N_2 and O_2 molecules enter the pores, but not the smaller cages and rings of the framework. The structure was then refined using the same model as in previous work using soft constraints on intratetrahedral Si-O and O-O distances and including some carbon atoms to

account for the residue arising from the calcination of the structure directing agent[15]. Reasonable agreement factors were obtained and the refined framework was used as the starting point for the MC molecular modelling to obtain a more meaningful structural model. The result from MC models were then used as starting points for the refinements at various pressures. It became clear that no improvement to the fits were obtained using individual diatomic molecules and thus the isoelectronic atoms were used in the refinements, Figure 4, to determine the centers of gravity of the diatomic molecules. The diatomic molecules in both systems partially occupy two sets of 4*a* Wyckoff sites (*x*,*y*,*z*) (Figures 5 and CIF files in SI). The exception is the low pressure point at 0.45 GPa in $Cmc2_1$ phase of O2-filled TON, in which a set of 4*a* Wyckoff sites (0,*y*,*z*) is occupied. These results are consistent with the Fourier difference maps.

A strong increase in the number of molecules per unit cell occurs up to 3 GPa for O_2 and N_2, pressure above which the occupancy saturates in both cases at 6 molecules per unit cell and thus 3 molecules per pore distributed with 75 % probability on four sites (Figure 6). The filling curve is slightly shifted to higher pressure for N_2. Less than full occupation of these sites could be partially related to the presence in the pores of a residue from the structure directing agent remaining after pyrolysis of the zeolite[15]. The higher intrusion pressure for nitrogen can be linked to its larger kinetic diameter and is in good agreement with the results of the simulations discussed below. The degree of filling is much greater than the saturation at 3.7 nitrogen molecules/UC[31] found by adsorption isotherm data. The filling data are similar to previous results for argon in terms of number of guest species per unit cell and much lower than the corresponding value of 12 for Ne, which has a significantly smaller kinetic diameter.

Figure 6 shows the simulated adsorption isotherms obtained for N_2 and O_2 at room temperature in TON. As mentioned above, the pressures selected for each gas in the GCMC simulations correspond to the experimental data points. The adsorbed amount of N_2 increases up to 5 N_2 molecules per unit cell upon increasing the pressure to ~3 GPa and then remains constant at about 5.5 N_2 per unit cell. In contrast, for O_2 in a similar pressure range, the adsorbed amount increases from about 4 O_2 molecules per unit cell to about 8 O_2 molecules per unit cell for increasing the pressure to $P < 2$ GPa and then decreases to about 6

O_2 molecules upon further increasing the pressure beyond $P > 2$ GPa. Even if O_2 has a slightly longer bond length than N_2, the larger maximum adsorbed amount for O_2 compared to N_2 can be explained by the slightly smaller Lennard-Jones size parameter for the former ($\sigma = 0.302$ for O_2 and $\sigma = 0.331$ nm for N_2). Overall, the behavior observed for these two gases can be rationalized as follows. At low pressures, upon compression, despite the observed unit cell volume decrease, the adsorbed amount increases as a result of the increasing gas chemical potential (we recall that at constant pressure the gas pressure and chemical potential are directly related). However, for large pressures, the unit cell compression prevails so that the volume accessible for adsorption – and hence the adsorbed amount – decreases. The strong increase followed by a decrease is not observed experimentally for the case of O_2-TON. This is probably due to kinetic factors as the filling curves are shifted to higher pressure in the experiments as compared to the simulations. The large increase followed by a decrease in the case of oxygen below 5 GPa in the MC simulations corresponds to the pressure range over which the oxygen is in the fluid state. Instead, at higher pressures good agreement is observed, and the number of molecules is constant or only decreases slightly at which the bulk N_2 and O_2 are solid. As a consequence, the relative volume remains systematically much higher and the compressibility lower than that of TON in non-penetrating pressure medium DAPHNE7474. As in the simulations, the filling curve of nitrogen is shifted to higher pressures with respect to that of oxygen due to its larger size.

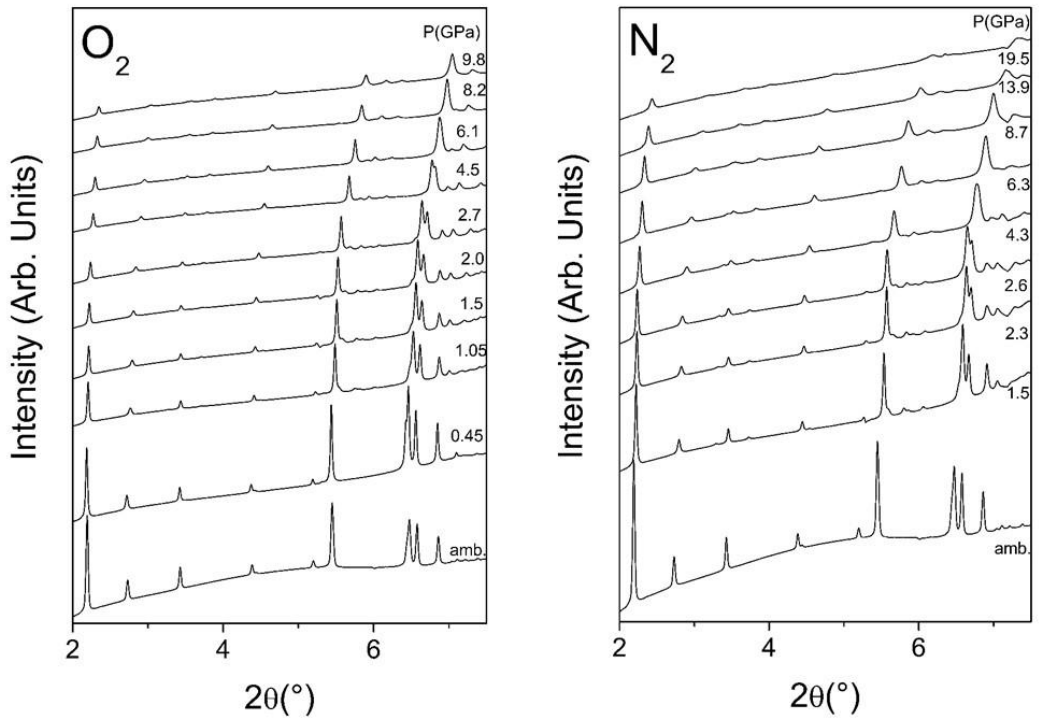

Figure 3. X-ray diffraction patterns of TON in O_2 and N_2 as a function of pressure (λ=0.41121 Å). The diffraction lines of ε-O_2 and ε-N_2 were observed above 10 GPa at diffraction angles above 8°. They exhibited strong texture and were typically more than an order of magnitude higher in intensity than the diffraction lines of TON indicating that the latter was completely immersed in a large amount of bulk O_2 or N_2 pressure transmitting medium

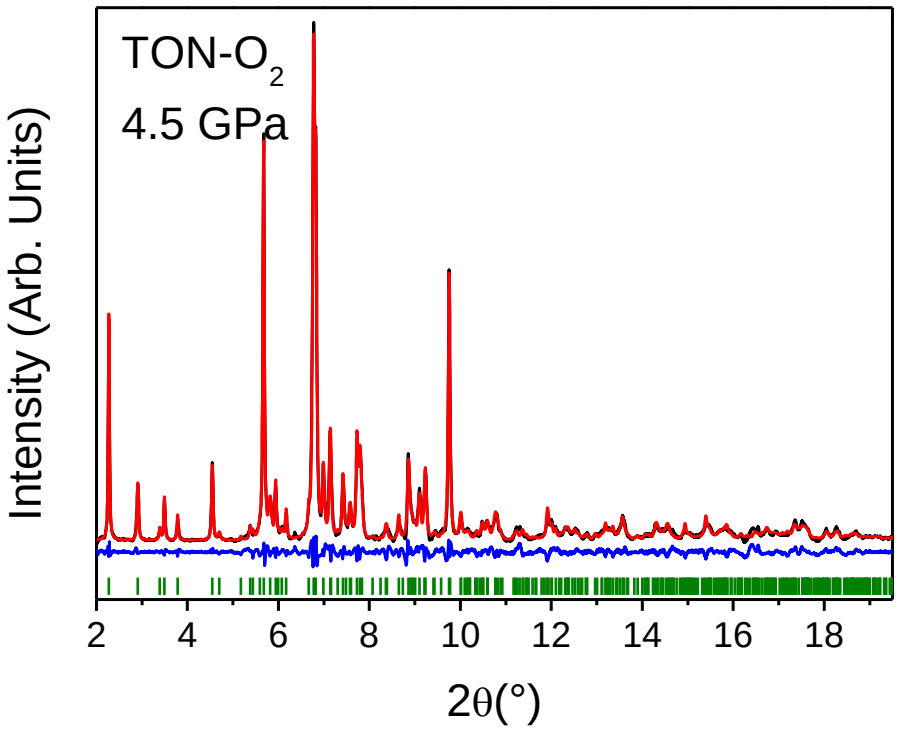

Figure 4. Experimental (black), calculated (red) and difference (blue) profiles for the the *Pbn*2_1 structure of TON-O_2 at 4.5(1) GPa. Vertical bars indicate the calculated positions of the Bragg reflections. The strong background due to Compton scattering from the diamond and broad features due to fluid O_2 have been subtracted.

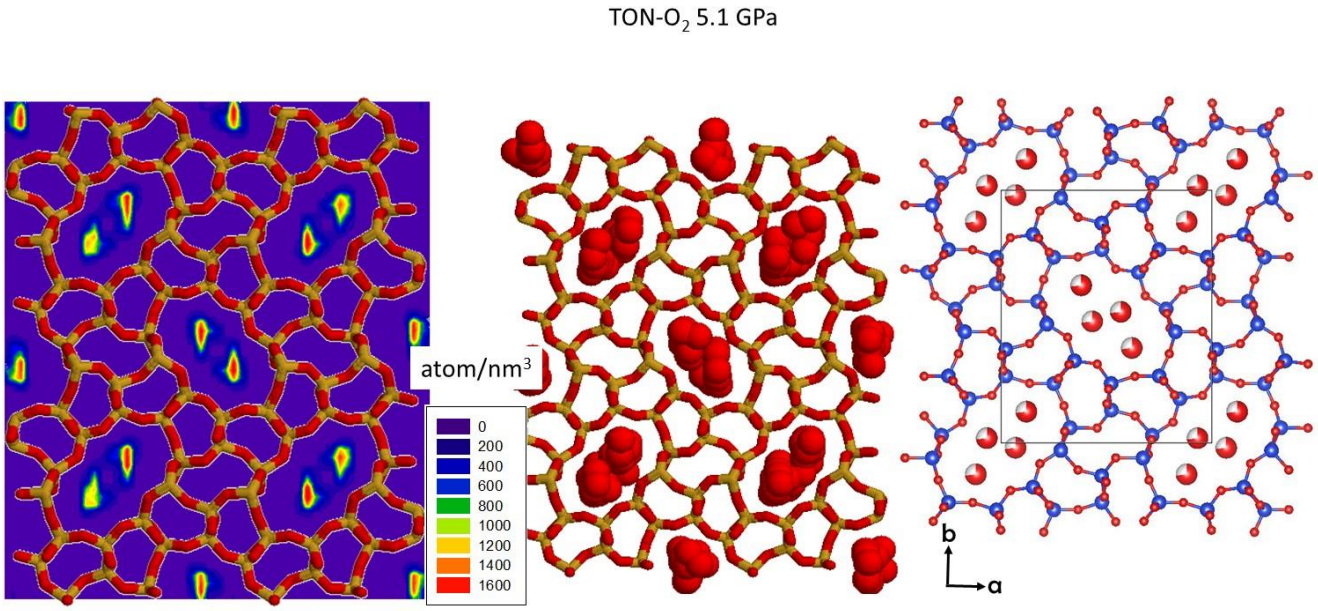

Figure 5. Density map (left) and projection of several unit cells along *z* (center) from MC modelling and the refined crystal structure of O_2-filled TON at 5.1 GPa (*Pbn*2_1) (right). Blue and red spheres represent the silicon and oxygen atoms in the zeolite, respectively. The large red spheres are the O atoms of the inserted O_2 molecules. Large red spheres in the figure at the right represent spherically disordered oxygen molecules and the shading represents the occupancy. The pore volume at 5.1 GPa, which is filled by O_2, is about 25Å^3/O_2 taking into account site occupancy of O_2 of 74%. This yields an O_2 density in the pores close to that of solid β–O_2 at similar pressures[45].

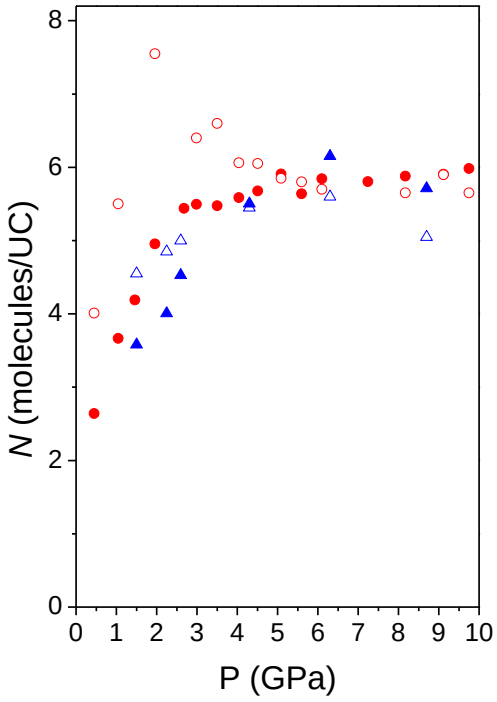

Figure 6. Experimental (solid symbols) and simulated (open symbols) adsorption isotherms for O_2 (red circles) and N_2 (blue triangles) at room temperature. Error bars are smaller than the symbol size. These data were obtained using GCMC simulations for a TON structure made up of 2 × 2 × 5 unit cells. For each pressure, the unit cell parameters (*a*, *b*, and *c*) in the simulation were taken from the experimental data.

Pore filling has a major effect on the compressibility of TON (Figure 7). The compressibility of TON is significantly lower in N_2 and O_2 than for empty TON[15]. The values for the cell parameters and volume are slightly lower in N_2 as compared to O_2 below 3 GPa due to the lower degree of filling of N_2 up to this pressure. A similar effect is seen in argon. The compressibility is greater than in the case of neon, which fills TON to a much greater extent. In all cases filled TON compresses to a much lesser degree than empty TON as could be expected.

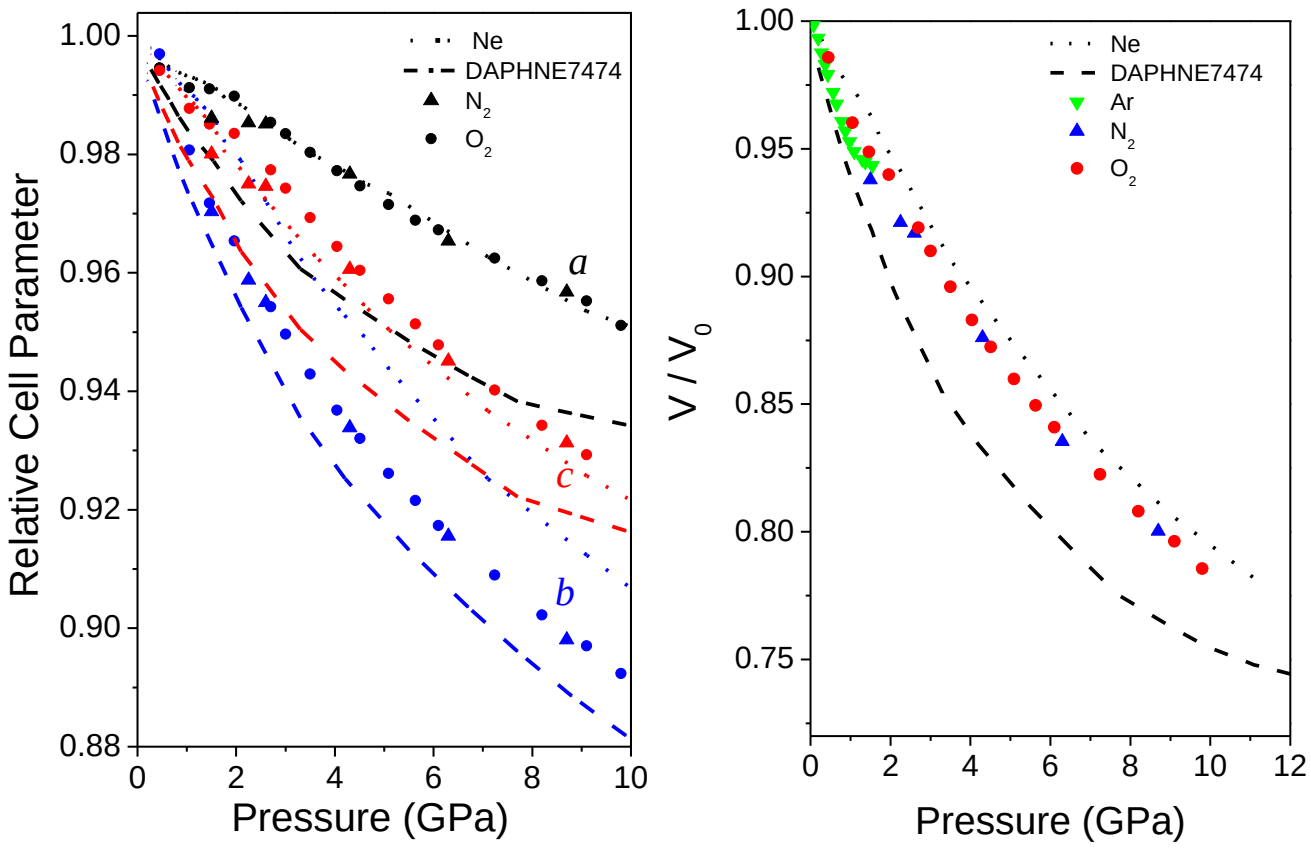

Figure 7. Relative cell parameters and volume (V/V_0) of TON in N_2, O_2 and Ar (V/V_0)[10] as a function of pressure (solid symbols). Dotted and dashed lines represents the behavior of TON in Ne[10] and DAPHNE7474[15], respectively. Error bars are smaller than the symbol size.

Compression is highly anisotropic with the **a** direction being particularly stiff (Figure 7) in all filled systems including neon. Compressibility along **c** is also similar to that observed in Ne. The compressibility along **b** is much greater in N_2 and O_2. This can be linked to the high distortion in the *xy* plane due to pore collapse, which is shifted to significantly higher pressure in neon due to the higher degree of filling. Pore collapse measured by changes in pore ellipticity is similar in all systems except neon, including empty TON (Figure 8).

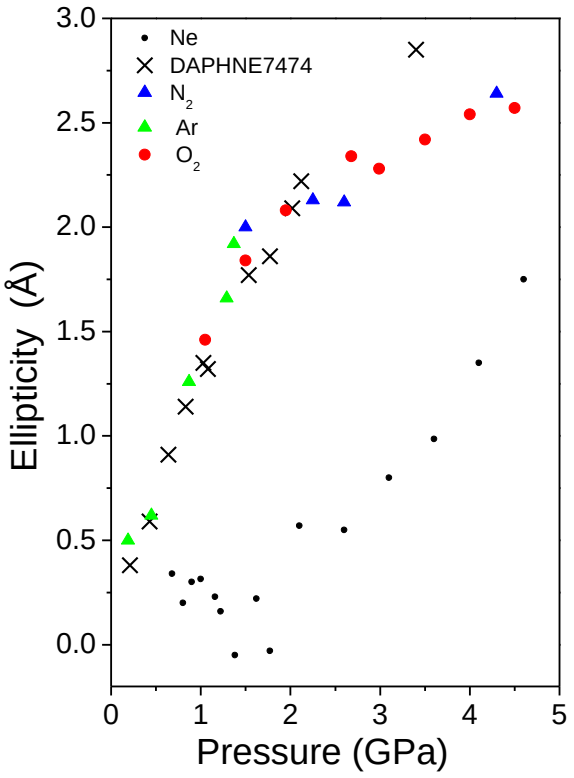

Figure 8. Pore ellipticity (difference between maximum and minimum diameters of the elliptical pores in TON) as a function of pressure of TON in N_2 and O_2, Ne[10], Ar[10] and DAPHNE7474[15]. Error bars are smaller than the symbol size.

MC simulations can provide further insight concerning the orientations of the inserted guest molecules. Following previous studies on nanoconfined fluids[46-47], we calculated the angular distribution $P(\cos\theta)$ for O_2 and N_2 confined in TON at room temperature where θ is the angle between the molecule axis and the z-axis (this axis corresponds to the channel axis in TON). As shown in Fig. 9, for O_2, a non-monotonous behavior is observed. O_2 does not show any preferential orientation at the lowest pressure, suggesting that the cavities are large enough to allow for large orientational diffusion. Upon increasing the pressure (from ~2 to ~5 GPa), the confined O_2 exhibits a preferred orientation, $\cos\theta \sim 0$, with their axis that tends to be perpendicular to the channel axis in TON (z-axis). As the pressure keeps increasing (> 6 GPa), the cavities become smaller and smaller and a bimodal angular distribution is observed. In this regime, more

and more molecules tend to be aligned with the channel axis (cos θ ~ 0.8-0.9), the other molecules exhibit a second preferential orientation with cos θ ~ 0 (perpendicular to the pore axis). Interestingly, the data shown in Fig. 9 suggest that a similar scenario is observed for N_2 confined in TON, but orientational features are less pronounced compared to O_2. At the lowest pressure, like for O_2, the N_2 molecules do not display a significantly marked angular distribution (even if a slightly preferred orientation with their axis perpendicular to the channel axis seems to be observed, i.e. cos θ ~ 0). Upon increasing the pressure from 2 to 6 GPa, the confined N_2 exhibits a preferred orientation with cos θ ~ 0.8 GPa. If the pressure is further increased (> 6 GPa), as observed for O_2, N_2 exhibits a bimodal angular distribution with a large number of molecules aligned perpendicular to the channel axis (cos θ ~ 0) and a non-negligible number of molecules with cos θ ~ 0.8.

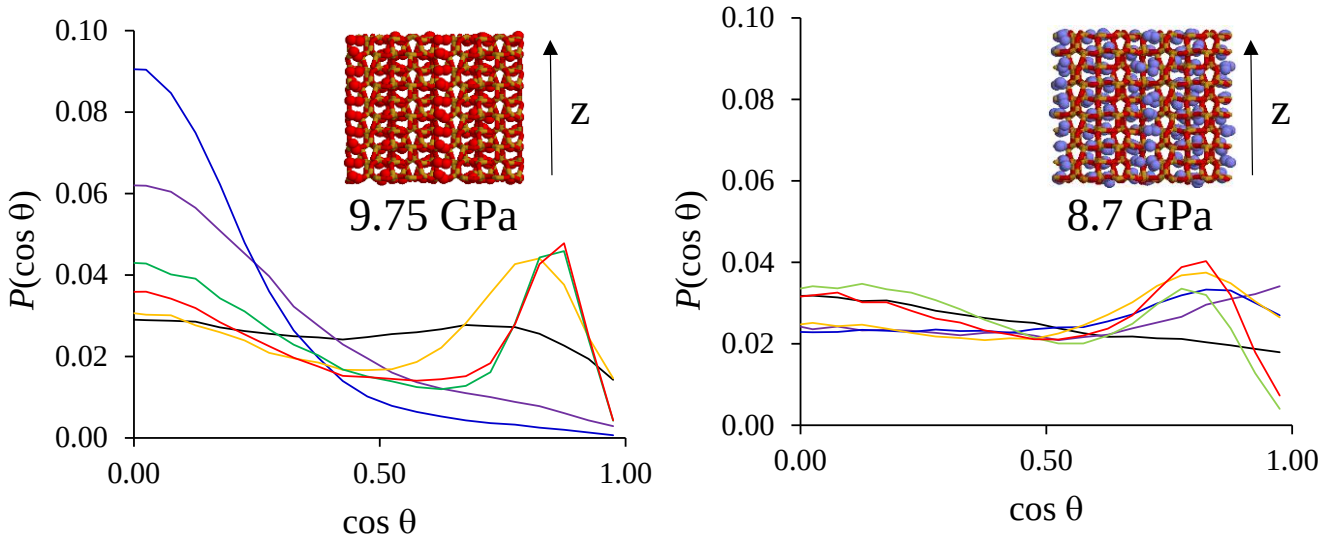

Figure 9. Simulated angular distributions $P(\cos\theta)$ for O_2 (*left*) and N_2 (*right*) confined in TON at room temperature and different pressure. θ is the angle between the molecule axis and the z-axis which corresponds to the channel axis in TON. For O_2, the color code is P = 1.05 GPa (black), 1.95 GPa (purple), 3.5 GPa (blue), 5.09 GPa (orange), 8.17 GPa (green), and 9.75 GPa (red). For N_2, the color code is 1.5 GPa (black), 2.25 GPa (purple), 2.6 GPa (blue), 4.3 GPa (orange), 6.3 GPa (green), and 8.7 GPa (red). For each gas, we also show a typical molecular configuration with the same color code as in Fig. 5 (the red and blue spheres are the O and N atoms in O_2 and N_2, respectively).

4. Conclusions

Strong agreement was observed between the results of Raman spectroscopy and X-ray diffraction in terms of pore filling and the presence of two sites for the diatomic molecules, which exhibit a significant degree of orientational disorder. The filling curve in nitrogen is shifted to slightly higher pressure due to its larger kinetic diameter. MC modelling indicates that as a function of pressure, the orientational distribution of the O_2 molecules exhibit the following sequence - isotropic-perpendicular to the channel axis-bimodal, whereas for N_2 it is isotropic-parallel to the channel axis-bimodal, but less pronounced. TON is an ideal model system to study confined O_2 and N_2 due to its 1D pore system and its relatively small unit cell for a zeolite. The observed filling behavior of O_2 and N_2 could be expected to be somewhat similar in more complex 3D systems such as MFI[9], although the larger pore diameter, the presence of two types of pores and channel intersections in this 3D system could favor a higher degree of disorder.

ASSOCIATED CONTENT

Supporting Information. Crystallographic information files (CIF) file containing the structural data for the N_2-TON system at 4.3 and the O_2-TON system at 4.5 have been supplied as supporting information. This material is available free of charge via the Internet at http://pubs.acs.org.

AUTHOR INFORMATION

Corresponding Author

*Julien Haines

Julien.Haines@umontpellier.fr

Author Contributions

The manuscript was written through contributions of all authors. All authors have given approval to the final version of the manuscript.

Notes

The authors declare no competing financial interests.

ACKNOWLEDGMENT

We acknowledge funding from the Italian Ministry of Education, Universities and Research, MIUR PRIN project ZAPPING, number 2015HK93L7. We also thank the Deep Carbon Observatory (DCO) initiative under the project Physics and Chemistry of Carbon at Extreme Conditions and the Ente Cassa di Risparmio di Firenze under the project Firenze Hydrolab 2. K.D. acknowledges the Polish Ministry of Science and Higher Education for financial support through the "Mobilność Plus" program. Some of the computations in this paper were performed using the Froggy platform of the GRICAD infrastructure (https://gricad.univ-grenoble-alpes.fr), which is supported by the Rhône-Alpes region (GRANT CPER07-13 CIRA) and the Equip@Meso project (reference ANR-10-EQPX-29-01) of the programme Investissements d'Avenir supervised by the Agence Nationale de la Recherche.

‖ Present address: Department of Chemistry and INSTM, University of Pavia, Viale Taramelli 16, Pavia 27100, Italy

REFERENCES

1. Haines, J.; Cambon, O.; Levelut, C.; Santoro, M.; Gorelli, F.; Garbarino, G., Deactivation of Pressure-Induced Amorphization in Silicalite SiO_2 by Insertion of Guest Species. *J. Am. Chem. Soc.* 2010, *132*, 8860-8861.

2. Coasne, B.; Haines, J.; Levelut, C.; Cambon, O.; Santoro, M.; Gorelli, F.; Garbarino, G., Enhanced Mechanical Strength of Zeolites by Adsorption of Guest Molecules. *Phys. Chem. Chem. Phys.* 2011, *13*, 20096-20099.

3. Santoro, M.; Gorelli, F.; Haines, J.; Cambon, O.; Levelut, C.; Garbarino, G., Silicon Carbonate Phase Formed from Carbon Dioxide and Silica under Pressure. *Proc. Natl. Acad. Sci. USA* 2011, *108*, 7689-7692.

4. Sartbaeva, A.; Haines, J.; Cambon, O.; Santoro, M.; Gorelli, F.; Levelut, C.; Garbarino, G.; Wells, S. A., Flexibility Windows and Compression of Monoclinic and Orthorhombic Silicalites. *Phys. Rev. B* 2012, *85,* 064109.

5. Santoro, M.; Gorelli, F. A.; Bini, R.; Haines, J.; van der Lee, A., High-Pressure Synthesis of a Polyethylene/Zeolite Nano-Composite Material. *Nat. Commun.* 2013, *4*, 1557.

6. Scelta, D.; Ceppatelli, M.; Santoro, M.; Bini, R.; Gorelli, F. A.; Perucchi, A.; Mezouar, M.; van der Lee, A.; Haines, J., High Pressure Polymerization in a Confined Space: Conjugated Chain/Zeolite Nanocomposites. *Chem. Mater.* 2014, *26*, 2249-2255.

7. Santoro, M. M.; Dziubek, K.; Scelta, D.; Ceppatelli, M.; Gorelli, F. A.; Bini, R.; Thibaud, J.-M.; Di Renzo, F.; Cambon, O.; Rouquette, J.; et al., High Pressure Synthesis of All-Transoid Polycarbonyl $[—(C═O)—]_n$ in a Zeolite. *Chem. Mater.* 2015, *27*, 6486-6489.

8. Santoro, M.; Scelta, D.; Dziubek, K.; Ceppatelli, M.; Gorelli, F. A.; Bini, R.; Garbarino, G.; Thibaud, J.-M.; Di Renzo, F.; Cambon, O.; et al., Synthesis of 1d Polymer/Zeolite Nanocomposites under High Pressure. *Chem. Mater.* 2016, *28*, 4065-4071.

9. Santoro, M.; Gorelli, F. A.; Bini, R.; Haines, J., Intermolecular Interactions in Highly Disordered, Confined Dense N_2. *J. Phys. Chem. Lett.* 2017, *8*, 2406-2411.

10. Thibaud, J. M.; Rouquette, J.; Dziubek, K.; Gorelli, F. A.; Santoro, M.; Garbarino, G.; Clement, S.; Cambon, O.; van der Lee, A.; Di Renzo, F.; et al., Saturation, of the Siliceous Zeolite TON with Neon at High Pressure. *J. Phys. Chem. C* 2018, *122*, 8455-8460.

11. Xu, W.; Liu, X. D.; Pena-Alvarez, M.; Jiang, H. C.; Dalladay-Simpson, P.; Coasne, B.; Haines, J.; Gregoryanz, E.; Santoro, M., High-Pressure Insertion of Dense H_2 into a Model Zeolite. *J. Phys. Chem. C* 2021, *125*, 7511-7517.

12. Coasne, B.; Czwartos, J.; Sliwinska-Bartkowiak, M.; Gubbins, K. E., Effect of Pressure on the Freezing of Pure Fluids and Mixtures Confined in Nanopores. *J. Phys. Chem. B* 2009, *113*, 13874-13881.

13. Long, Y.; Palmer, J. C.; Coasne, B.; Sliwinska-Bartkowiak, M.; Gubbins, K. E., Under Pressure: Quasi-High Pressure Effects in Nanopores. *Micropor. Mesopor. Mat.* 2012, *154*, 19-23.

14. Barri, S. A. I.; Smith, G. W.; White, D.; Young, D., Structure of Theta-1, the First Unidimensional Medium-Pore High-Silica Zeolite. *Nature* 1984, *312*, 533-534.

15. Thibaud, J. M.; Rouquette, J.; Hermet, P.; Dziubek, K.; Gorelli, F. A.; Santoro, M.; Garbarino, G.; Alabarse, F. G.; Cambon, O.; Di Renzo, F.; et al., High-Pressure Phase Transition, Pore Collapse, and Amorphization in the Siliceous 1d Zeolite, TON. *J. Phys. Chem. C* 2017, *121*, 4283-4292.

16. Gregoryanz, E.; Goncharov, A. F.; Sanloup, C.; Somayazulu, M.; Mao, H. K.; Hemley, R. J., High P-T Transformations of Nitrogen to 170 GPa. *J. Chem. Phys.* 2007, *126* 184505.

17. Freiman, Y. A.; Jodl, H. J., Solid Oxygen. *Phys. Rep.* 2004, *401*, 1-228.

18. Freiman, Y. A.; Jodl, H. J.; Crespo, Y., Solid Oxygen Revisited. *Phys. Rep.* 2018, *743*, 1-55.

19. Reichlin, R.; Schiferl, D.; Martin, S.; Vanderborgh, C.; Mills, R. L., Optical Studies of Nitrogen to 130-GPa. *Phys. Rev. Lett.* 1985, *55*, 1464-1467.

20. Bini, R.; Jordan, M.; Ulivi, L.; Jodl, H. J., Infrared and Raman Studies on High Pressure Phases of Solid N_2: An Intermediate Structural Modification between Epsilon and Delta Phases. *J. Chem. Phys.* 1998, *108*, 6849-6856.

21. Olijnyk, H.; Jephcoat, A. P., Vibrational Dynamics of Isotopically Dilute Nitrogen to 104 GPa. *Phys. Rev. Lett.* 1999, *83*, 332-335.

22. Bini, R.; Ulivi, L.; Kreutz, J.; Jodl, H. J., High-Pressure Phases of Solid Nitrogen by Raman and Infrared Spectroscopy. *J. Chem. Phys.* 2000, *112*, 8522-8529.

23. Gregoryanz, E.; Goncharov, A. F.; Hemley, R. J.; Mao, H. K.; Somayazulu, M.; Shen, G. Y., Raman, Infrared, and X-Ray Evidence for New Phases of Nitrogen at High Pressures and Temperatures. *Phys. Rev. B* 2002, *66,* 224108.

24. Frost, M.; Howie, R. T.; Dalladay-Simpson, P.; Goncharov, A. F.; Gregoryanz, E., Novel High-Pressure Nitrogen Phase Formed by Compression at Low Temperature. *Phys. Rev. B* 2016, *93,* 024113.

25. Goncharov, A. F.; Crowhurst, J. C.; Struzhkin, V. V.; Hemley, R. J., Triple Point on the Melting Curve and Polymorphism of Nitrogen at High Pressure. *Phys. Rev. Lett.* 2008, *101,* 095502.

26. Goncharov, A. F.; Gregoryanz, E.; Mao, H. K.; Liu, Z. X.; Hemley, R. J., Optical Evidence for a Nonmolecular Phase of Nitrogen above 150 GPa. *Phys. Rev. Lett.* 2000, *85*, 1262-1265.

27. Gregoryanz, E.; Goncharov, A. F.; Hemley, R. J.; Mao, H. K., High-Pressure Amorphous Nitrogen. *Phys. Rev. B* 2001, *64,* 052103.

28. Eremets, M. L.; Hemley, R. J.; Mao, H.; Gregoryanz, E., Semiconducting Non-Molecular Nitrogen up to 240 GPa and Its Low-Pressure Stability. *Nature* 2001, *411*, 170-174.

29. Eremets, M. I.; Gavriliuk, A. G.; Trojan, I. A.; Dzivenko, D. A.; Boehler, R., Single-Bonded Cubic Form of Nitrogen. *Nat. Mater.* 2004, *3*, 558-563.

30. Tomasino, D.; Kim, M.; Smith, J.; Yoo, C. S., Pressure-Induced Symmetry-Lowering Transition in Dense Nitrogen to Layered Polymeric Nitrogen (Lp-N) with Colossal Raman Intensity. *Phys. Rev. Lett.* 2014, *113,* 205502.

31. Direnzo, F.; Remoue, F.; Massiani, P.; Fajula, F.; Figueras, F., Influence of Diffusional Barriers on the Thermal-Analysis of the Zeolite TON *Thermochim Acta* 1988, *135*, 359-364.

32. Di Renzo, F.; Remoué, F.; Massiani, P.; Fajula, F.; Figueras, F.; Descourières, T., Crystallization Kinetics of Zeolite TON. *Zeolites* 1991, *11*, 539-548.

33. Mao, H. K.; Xu, J.; Bell, P. M., Calibration of the Ruby Pressure Gauge to 800 Kbar under Quasi-Hydrostatic Conditions. *J. Geophys. Res.: Solid Earth* 1986, *91*, 4673-4676.

34. Ceppatelli, M.; Gorelli, F. A.; Haines, J.; Santoro, M.; Bini, R., Probing High-Pressure Reactions in Heterogeneous Materials by Raman Spectroscopy. *Z. Krist.-Cryst. Mater.* 2014, *229*, 83-91.

35. Hammersley, A. P.; Svensson, S. O.; Hanfland, M.; Fitch, A. N.; Hausermann, D., Two-Dimensional Detector Software: From Real Detector to Idealised Image or Two-Theta Scan. *High Pressure Res.* 1996, *14*, 235-248.

36. Rodriguez-Carvajal, J., Magnetic Structure Determination from Powder Diffraction Using the Program Fullprof. *Applied Crystallography* 2001, 30-36.

37. Momma, K.; Izumi, F., Vesta 3 for Three-Dimensional Visualization of Crystal, Volumetric and Morphology Data. *J. Appl. Crystallogr.* 2011, *44*, 1272-1276.

38. Alabarse, F. G.; Rouquette, J.; Coasne, B.; Haidoux, A.; Paulmann, C.; Cambon, O.; Haines, J., Mechanism of H_2O Insertion and Chemical Bond Formation in $AlPO_4$-54·xH_2O at High Pressure. *J. Am. Chem. Soc.* 2015, *137*, 584-587.

39. Desbiens, N.; Boutin, A.; Demachy, I., Water Condensation in Hydrophobic Silicalite-1 Zeolite: A Molecular Simulation Study. *J. Phys. Chem. B* 2005, *109*, 24071-24076.

40. Coasne, B.; Weigel, C.; Polian, A.; Kint, M.; Rouquette, J.; Haines, J.; Foret, M.; Vacher, R.; Ruffle, B., Poroelastic Theory Applied to the Adsorption-Induced Deformation of Vitreous Silica. *J. Phys. Chem. B* 2014, *118*, 14519-14525.

41. Potoff, J. J.; Siepmann, J. I., Vapor-Liquid Equilibria of Mixtures Containing Alkanes, Carbon Dioxide, and Nitrogen. *AICHE J.* **2001**, *47*, 1676-1682.

42. Zhang, L.; Siepmann, J. I., Direct Calculation of Henry's Law Constants from Gibbs Ensemble Monte Carlo Simulations: Nitrogen, Oxygen, Carbon Dioxide and Methane in Ethanol. *Theor. Chem. Acc.* **2006**, *115*, 391-397.

43. Carré, A.; Horbach, J.; Ispas, S.; Kob, W., New Fitting Scheme to Obtain Effective Potential from Car-Parrinello Molecular-Dynamics Simulations: Application to Silica. *Epl-Europhys Lett* **2008**, *82*, No. 17001.

44. Santoro, M.; Dziubek, K.; Scelta, D.; Morana, M.; Gorelli, F. A.; Bini, R.; Hanfland, M.; Rouquette, J.; Di Renzo, F.; Haines, J., Dense, Subnano Phase of Clustered O_2. *J. Phys. Chem. C* 2019, *123*, 9651-9657.

45. Fujihisa, H.; Akahama, Y.; Kawamura, H.; Ohishi, Y.; Shimomura, O.; Yamawaki, H.; Sakashita, M.; Gotoh, Y.; Takeya, S.; Honda, K., O-8 Cluster Structure of the Epsilon Phase of Solid Oxygen. *Phys. Rev. Lett.* **2006**, *97,* 085503

46. Coasne, B.; Alba-Simionesco, C.; Audonnet, F.; Dosseh, G.; Gubbins, K. E., Adsorption, Structure and Dynamics of Benzene in Ordered and Disordered Porous Carbons. *Phys. Chem. Chem. Phys.* 2011, *13*, 3748-3757.

47. Coasne, B.; Fourkas, J. T., Structure and Dynamics of Benzene Confined in Silica Nanopores. *J. Phys. Chem. C* 2011, *115*, 15471-15479.

TOC Graphic